Journal of Thermal Science Vol.32, No.4 (2023) 1501−1511

https://doi.org/10.1007/s11630-023-1819-6 **Article ID: 1003-2169(2023)04-1501-11**

Temperature Fluctuation of a Closed-Cycle Helium Joule-Thomson Cryocooler with Two-Stage Precooling

CHEN Zhichao[1,2], CUI Xiaoyu[1], LIU Shaoshuai[2*], WU Yinong[2*], JIANG Zhenhua[2], DING Lei[1,2]

1. School of Energy and power Engineering, University of Shanghai for Science and Technology, Shanghai 20093, China
2. Shanghai Institution of Technology and Physics, Chinese Academy of Sciences, Shanghai 200083, China

Abstract: For quantum communications, single-photon detection, millimeter wave detection and other space projects, all of them need to work at liquid helium temperatures to achieve excellent performance. The closed-cycle helium Joule-Thomson cryocooler (JTC) is currently one of the mainstream solutions to realize the liquid helium temperature. While realizing the liquid helium temperature, the detector has strict requirements on the temperature fluctuation of the JTC, because the thermal noise caused by the JTC temperature fluctuation will have a critical impact on the detection performance. The typical closed-cycle helium JTC is precooling by a two-stage precooler. When the operating parameters of the JTC compressor remain unchanged, the change of the precooler is the main factor that affects the temperature fluctuation of the JTC. To explore the influence mechanism of JTC temperature fluctuations, experimental and theoretical studies are carried out. Based on the real gas equation of state, the influence of various parameters on the evaporator temperature fluctuations is explained. Research results show that the increase in temperature of each stage will cause the temperature of the JTC to increase. Especially, the change of the secondary precooling temperature (T_{pre2}) has the most obvious influence on JTC temperature. Furthermore, the influence of the JT compressor's buffer tank volume V_b on temperature fluctuation is studied. By increasing the V_b, the JTC temperature fluctuation caused by the temperature change of the precooler can be effectively reduced.

Keywords: temperature fluctuation, liquid helium temperature, Joule-Thomson cryocooler, precooling temperature

1. Introduction

Some satellite detectors need to work in the liquid helium temperature to obtain higher accuracy and wider detection range [1–3]. The Joule-Thomson cryocooler (JTC) has replaced the liquid helium Dewar and has become one of the mainstream solutions for space cryocooler in liquid helium temperature due to its significant advantages (long life, low weight, long-distance deployment, etc.). In fact, most space detectors

Received: Sep 16, 2021
AE: HAN Xiaohong
Corresponding author: LIU Shaoshuai; WU Yinong
E-mail: liushaoshuai@mail.sitp.ac.cn wyn@mail.sitp.ac.cn
www.springerlink.com

Nomenclature

A	aera/m^2	X	quality
Cp	heat capacity/$J\cdot(kg\cdot K)^{-1}$	**Greek symbols**	
h	specific enthalpy/$kJ\cdot kg^{-1}$	λ	thermal conductivity/$W\cdot(m\cdot K)^{-1}$
n	the amount of substance/mol	ρ	density/$kg\cdot m^{-3}$
P	pressure/MPa	τ	time/s
Q	cooling power/mW	**Subscripts**	
q_m	mass flow rate/$mg\cdot s^{-1}$	b	buffer tank
R	universal gas constant, 8.314 J/(mol·K)	e	JTC evaporator
T	temperature/K	H, L	high-pressure and low-pressure side
u	velocity/$mg\cdot s^{-1}$	i	i-th micro-element
V	volume/m^3	pre	precooler

launched in recent years and in the future, use JTC to achieve liquid helium temperature. The Planck satellite launched in May 2009 used a 4 K JTC developed by Rutherford Appleton Laboratory (RAL) to cool its High-Frequency Instrument (HFI). As of April 2013, the JTC is still working normally, which marks the first realization of the liquid helium temperature JTC's long-life on-orbit operation [4, 5]. In addition, the SPCIA satellite developed by JAXA and the JWST satellite developed by NASA both use JTC to cool their core detectors to liquid helium temperature [6, 7].

The JTC evaporator is the core component that couples with the detector and provides the cooling capacity of liquid helium temperature. However, the detector also has further requirements on the temperature fluctuation of the JTC evaporator when it works in the liquid helium temperature. According to Planck's on-orbit data analysis, Lamarre et al. pointed out that the HFI bolometer and acquisition system onboard is extremely stable essentially, and the instability that affects the HFI detection results is mainly caused by temperature fluctuations [8]. To perform long-term integral observation of weak detection objects, the Mid-Infrared Instrument (MIRI) of JWST satellite must be cooled to 6 K while maintaining the temperature fluctuations of the detector stable. The indicators of 6 K stage temperature fluctuation are 0.1 K@10 000 s and 0.25 K@24 h, respectively [9]. Orlowska A.H. et al. have developed a 2.5 K–4 K JTC prototype suitable for space applications. The ground test results show that the temperature fluctuation of the JTC evaporator within 70 hours does not exceed 30 mK, and T_{pre2} changed by 0.7 K [10]. Inatani J. et al. reported the performance of a JTC used to cool a sub-millimeter SIS hybrid receiver in space application. In the experimental test, the temperature fluctuations of each stage within 20 minutes were 6 mK@4 K and 0.3 K@20 K, 0.7 K@100 K. At the same time, the ambient temperature changed by 0.4 K. The influence of temperature changes at each stage on the temperature changes of the JTC evaporator remains to be explained [11]. Narasaki K. et al. further optimized the JTC developed by Inatani J. The test results showed that the temperature fluctuations at each stage within 10 minutes were 7 mK@4 K, 50 mK@20 K, 0.15 K@100 K, and the ambient temperature changed by 0.8 K. There is a certain correlation between the JTC evaporator temperature and the ambient temperature [12]. The test results of the cryostat in ATHENA by Prouvé T. et al. showed that when the secondary cold head of the pre-cooler did not take temperature control measures, the temperature of the secondary cold head increased by 0.1 K, and the temperature of the JTC evaporator increased by 7 mK. The magnitude of this change is equivalent to the magnitude of the impact of environmental temperature changes [13]. The experimental data of the above research shows that the temperature fluctuation of the JTC evaporator is related to the temperature changes at each stage, but there is no yet relevant research on the factors affecting the temperature fluctuation of the JTC evaporator.

From the previous research work, we can find that there are two kinds of temperature fluctuations in the JTC, namely, the high-frequency fluctuation of the short-term temperature and the low-frequency fluctuation of the long-term temperature [14]. According to the theories of the thermal resistance method to suppress temperature fluctuations, short-term temperature fluctuations can be suppressed by increasing the thermal resistance between the evaporator and the detector. Through this method, Hasegawa Y. et al. successfully controlled the short-term fluctuation of the cold head temperature of the cryocooler within 1 mK [15, 16]. However, it is difficult to suppress the fluctuation of the temperature over a long period of time by the above methods. The scheme commonly used to control the temperature of the cryocooler recently is to use PID algorithm [17, 18]. For cryocoolers such as pulse tube or Stirling, the cold head cooling capacity is provided by the

sensible heat of the working fluid, and the cold head temperature changes with the change of the PID control quantity. However, the cooling capacity of the evaporator of the JTC is provided by the latent heat of the helium, and the temperature of the cold head is not directly affected by the heat load, which increases the difficulty of the temperature control of the JTC evaporator. Although we can easily control the temperature of the JTC evaporator by adjusting the low pressure of the JTC compressor unit, there are still some unsolved problems in the regulation of multistage JTC compressor unit, such as the compressor piston offset [19]. Therefore, it is easier to obtain the method of indirectly suppress the temperature fluctuation by clarifying the factors that affect the temperature fluctuation of the JTC evaporator.

Based on the two-stage Gifford-McMahon (GM) cryocooler precooling the JTC, this paper carried out an experimental study on the temperature fluctuation of the JTC evaporator, clarifying the influencing factors of the JTC evaporator temperature fluctuation through theoretical analysis of the temperature and pressure in the JTC.

2. Experimental Setup

The experimental setup is shown in Fig. 1. The structure is a typical space-application helium JTC. The core components include the JT compressor unit, three counterflow heat exchangers (CHX), two precooling heat exchangers (PHX), a throttling element, an evaporator, and a bypass pipeline. The high-pressure room-temperature helium gas discharged from the JT compressor unit is pre-cooled by CHX1, PHX1, CHX2, PHX2, and CHX3. The temperature of working fluid then drops below the inversion temperature (about 45 K for helium-4). Then the helium gas is throttled to the two-phase state through a throttling element. Liquid helium absorbs heat by phase change in the evaporator, providing cooling capacity at liquid helium temperature. Finally, the low-temperature helium gas flows back to the JTC compressor through CHX3, CHX2, and CHX1, and cools the income high-temperature helium gas. A bypass pipeline is set up in this experiment for rapid cooling of the JTC. Initially the temperature of the final stage (which composes of CHX3, throttling element and evaporator) is greater than the inversion temperature of helium in the initial stage of cooling. At this temperature, helium will have a heating effect after throttling. Without bypass pipeline, the heat generated by throttling will flow into the low-pressure pipeline of CHX3, and the net cooling capacity flow into the final stage will be reduced, which will greatly increase the cooling time of the final stage. The throttling element is a laser-etched orifice with diameter of about 30 μm. This structure is more compact comparing with capillary tube. But due to its small pore diameter, it is easy to be blocked by solid impurities in the pipeline. So, it is necessary to install a filter in the JT pipeline to prevent solid impurities. In addition, the impurity gas released by the material during the operation of the closed-cycle JTC will also block the throttle orifice after its solidification in the low temperature, so it is also necessary to add a getter to purify helium gas. CHXs are Linde-type heat exchanger, where high-pressure and low-pressure fluids flow in opposite directions in the heat exchanger, which can ensure high heat exchange efficiency (>97%) at a lower

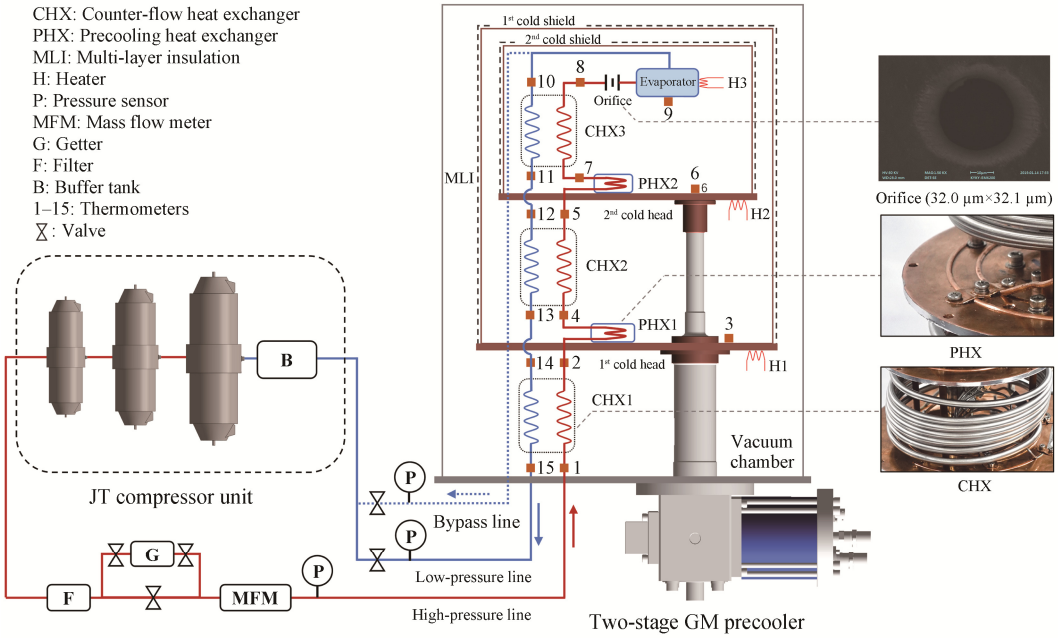

Fig. 1 Experimental setup of the two-stage GM precooled helium JTC

pressure drop. Among the JTC reported by other institutions, both annular space and circular space can be used as the low-pressure side [20, 21]. Considering the current processing capacity, we chose the annular space as the low-pressure side. PHX is an interference fit structure of the high-pressure round tube and the vortex groove on the cold head of the precooler, which can effectively reduce the contact thermal resistance. The precooling machine in this paper adopts two-stage GM cryocooler, and its secondary cold head has 1.5 W@4.2 K cooling performance. By heating the primary and secondary cold heads separately, the required temperature in the experiment can be reached. The above components at cryogenic temperature were placed in a high vacuum tank, which reduced the convection heat leakage during the experiment. At the same time, the copper cold shield installed at the first and second stages of the precooler are used to reduce radiation heat leakage, and the multi-layer insulation (MLI) is used to further reduce the effective emissivity of the cold shield surface and achieve lower heat leakage loss. All solid heat transfer contact surfaces in the experimental device are filled with thermal grease to obtain good thermal contact.

The temperature measurement points are shown in the small square dots 1–15 in the figure, which can obtain the inlet and outlet fluid temperature of each CHX. To reduce the temperature measurement error on the thin tube, a copper temperature measurement base is silver welded on the tube wall. The temperature sensor uses a Cernox thermometer, which has a temperature measurement accuracy of ±5 mK @ 4 K and ±16 mK @ 77 K respectively. And the accuracy of the data acquisition instrument is ±(0.1 Ω+0.04%Rd), so the final temperature measurement uncertainty is ±6.6 mK @ 4 K and ±96 mK @ 77 K respectively. The pressure sensors are respectively arranged in the high-pressure, low-pressure and bypass pipeline at room temperature. During the operation of the JTC, the bypass pipeline can act as a connecting pipe through which the evaporator pressure can be measured. The flowmeter used is a thermal mass flowmeter which has an accuracy of ±(0.5%Rd+0.1%FS). The simulated heat load H3 at the JTC evaporator is driven by a precision DC power supply. With the voltage and current of H3 measured through a four-wire method, the accurate heating amount can be obtained.

3. Experimental Results

After a complete cooling process, the temperature of the JTC evaporator (T_e) successfully reached the liquid helium temperature. The operating parameters of JTC are shown in Table 1.

The theoretical maximum cooling capacity of JTC is calculated as [22]:

$$\begin{aligned} Q &= q_m \times \min\left[\left(h_{(T_9, X=1)} - h_{(T_8, P_H)}\right), \left(h_{(T_7, P_L)} - h_{(T_7, P_H)}\right)\right] \\ &= q_m \times \left(h_{(T_9, X=1)} - h_{(T_8, P_H)}\right) \\ &= 13.7 \text{ mg/s} \times (20.9 - 9.4) \text{ kJ/kg} = 157.6 \text{ mW} \end{aligned} \quad (1)$$

where q_m represents the mass flow rate. To simulate the temperature fluctuation of the evaporator during the actual operation of the JTC, a heat load of 100 mW was applied to H3, and a 12 h long-term temperature fluctuation experiment was carried out. During the experiment, a constant heat flux is applied to the primary and secondary cold heads of GM cryocooler, and the temperature fluctuation of the cold head is affected by its own operating characteristics and the environment temperature. As shown in Fig. 2, the temperature fluctuations at each stage within 12 h are 47.20 mK@T_e, 2.09 K@T_{pre2}, 4.36 K@T_{pre1}, and 7.24 K@T_{atm}. It can be seen from the figure that the temperature at each stage shows an upward trend, and T_e has a certain correlation with the trend of temperature changes at each stage. Comparing the temperature curve of T_{pre2} and T_e, it can be found that the correlation between the two is relatively high, which indicating that the change of the T_{pre2} has a greater impact on T_e. The specific analysis is discussed in detail below.

Table 1 Operating parameters of the JTC

Items	Values
Senondary precooling temperature, T_{pre2} (T_7)	15 K
Throttling temperature, $T_{orifice}$ (T_8)	4.3 K
Evaporator temperature, T_e (T_9)	4.3 K
High-pressure, P_H	2.0 MPa
Low-pressure, P_L	0.11 MPa
Mass flow rate, q_m	13.7 mg/s

In the closed-cycle JTC, helium is mainly concentrated in the cold region. The temperature change of the cold region has a greater impact on the energy balance and the amount of substance contained in each node in the low-pressure pipeline. This is why T_{pre2} has a greater effect on T_e. As the temperature of the cold region increases, helium is not concentrated in the cold region, but is transferred to hot region or other region of the JTC. Similarly, when the temperature of the hot region increases, helium will also transfer to other regions. However, since the helium contained in the hot region is much less than that in the cold region, the temperature change in the hot region has a little effect on the energy balance and the amount of substance contained in each node. With the temperature of each region increasing, it means that the system average temperature increases, so the system pressure also increases with the increase of

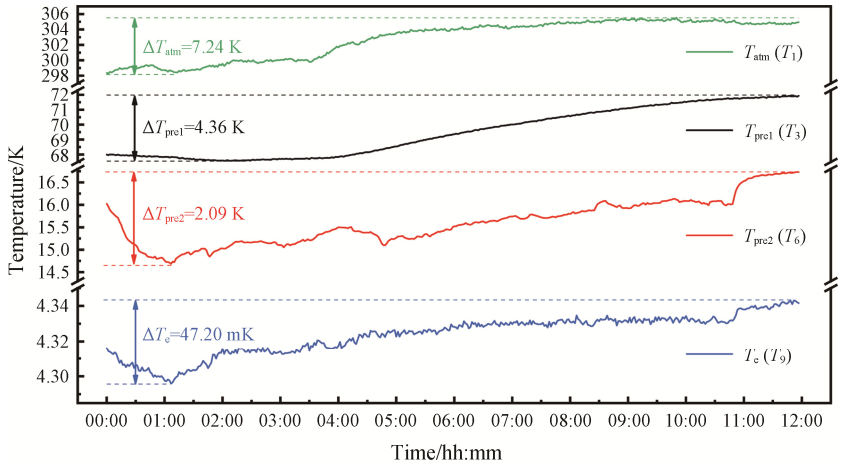

Fig. 2 Temperature fluctuations of each stage within 12 h, reprinted from Ref. [23]

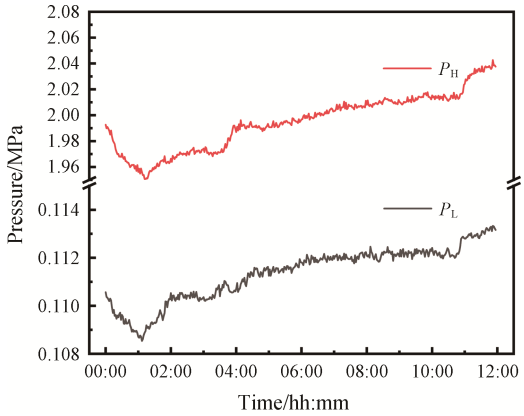

Fig. 3 Pressure fluctuations within 12 h

the density of each region. Fig. 3 shows the high-pressure (P_H) and low-pressure (P_L) curves of the JTC within 12 hours. From the figure, the P_H and P_L of JTC change over time, which is the same as the temperature change trend at each stage. According to the principle of the liquid helium temperature JTC, the saturation temperature corresponding to P_L in the low-pressure pipeline is the temperature of the JTC evaporator [22]. Therefore, the change of each stage in the JTC is by affecting P_L and subsequently the saturation temperature of the JTC evaporator.

4. Discussions

From the above analysis, we know that the temperature change of each stage will have an impact on the energy balance and the amount of substance contained in the JTC low-pressure pipeline. However, the temperature in the low-pressure pipeline is a non-linear distribution from 4–300 K, so in order to characterize the temperature distribution in the low-pressure pipeline and quantitatively analyze the superimposed influence of temperature changes at each stage, based on the ideal gas law, we use $\overline{T}_L$ to represent the average temperature of low-pressure temperature distribution, which is defined as follows:

$$\overline{T}_L = \frac{P_L V_L}{n_L R} \tag{2}$$

where R represents the universal gas constant, which is 8.314 J/(mol·K). Since the low-pressure drop is relatively small (2 kPa/110 kPa), the pressure change along the pipeline has little effect on the thermophysical properties of helium. To simplify the calculation, the influence of pressure drop of the pipeline is ignored.

However, the working temperature range of the low-pressure pipeline is 4–300 K. The non-ideal property of helium at low temperature increases significantly, which makes the calculation error of the ideal gas law too large [24]. So, it is necessary to introduce real gas equation of state for calculation. At present, Peng-Robinson equation of state is one of the most widely used in academia and industry because it offers relatively accurate results with practical computational usage [25]. The equations are as follows:

$$P = \frac{nRT}{V-nb} - \frac{a(T)n^2}{V(V+nb)+b(nV-n^2b)} \tag{3}$$

$$a(T) = 0.457\,24\frac{R^2T_c^2}{P_c}\left[1+K\left(1-\frac{T}{T_c}\right)^{0.5}\right]^2 \tag{4}$$

$$b = 0.077\,80\frac{RT_c}{P_c} \tag{5}$$

$$K = 0.374\,64 + 1.542\,26\omega - 0.269\,92\omega^2 \tag{6}$$

For helium: T_c=5.1953 K, P_c=0.227 61 MPa, ω=–0.390.

It can be seen from Eqs. (3)–(5) that in the Peng-Robinson equation of state, when V is known that $T(P, n)$ and $n(P, T, V)$ are implicit equations. For the

convenience of analysis, we define the two as $T=f(P, n)$, $n=V\cdot g(P, T)$.

Therefore, $\overline{T}_{\mathrm{L(real\text{-}gas)}}$ can be defined as:

$$\overline{T}_{\mathrm{L(real\text{-}gas)}} = f\left(P_{\mathrm{L}}, n_{\mathrm{L}}\right) \tag{7}$$

From Eq. (7) we can see that to calculate $\overline{T}_{\mathrm{L}}$ at a certain time, it is necessary to know the P_{L} and n_{L}. Due to the temperature distribution in the low-pressure pipeline, the n_{L} cannot be directly calculated. Therefore, it is necessary to divide the low-pressure pipeline into several micro-elements along the length and calculate the amount of substances in each micro-element separately. The amount of substance in the i-th micro-element is defined as:

$$\mathrm{d}n_i = V_i \cdot g\left(P_{\mathrm{L}}, T_i\right) \tag{8}$$

where T_i represent the temperature of the i-th micro-element.

So, the n_{L} is:

$$n_{\mathrm{L}} = \int_0^x \mathrm{d}n_i \mathrm{d}x = \int_0^x V_i \cdot g\left(P_{\mathrm{L}}, T_i\right)\mathrm{d}x = V_{\mathrm{L}} \cdot g\left(P_{\mathrm{L}}, T_i\right) \tag{9}$$

Substituting Eq. (9) into Eq. (7), the $\overline{T}_{\mathrm{L(real\text{-}gas)}}$ can be obtained as

$$\overline{T}_{\mathrm{L(real\text{-}gas)}} = f\left(P_{\mathrm{L}}, n_{\mathrm{L}}\right) = f\left[P_{\mathrm{L}}, V_{\mathrm{L}} \cdot g\left(P_{\mathrm{L}}, T_i\right)\right] \tag{10}$$

For closed cycle JTC, V_{L} is constant and can be calculated by designing size parameters, so the calculation of $\overline{T}_{\mathrm{L}}$ depends on P_{L} and T_i, where the low-pressure temperature distribution T_i is the key to calculating V_{L} and $\overline{T}_{\mathrm{L}}$. However, the heat capacity of helium in the 4–30 K temperature where CHXs work in the JTC has a large change. The temperature in the pipeline is nonlinearly distributed. Therefore, to obtain an accurate temperature distribution in the CHX, a flow and heat transfer model needs to be established.

4.1 Calculated temperature distribution of the JT cryocooler

CHX is the mostly commonly used heat exchanger for JTC, and many studies have used two-dimensional models to analyze its flow and heat transfer characteristics [26]. To simplify the calculation model, this article makes the following assumptions:

(1) Pressure drop only occurs in the JT orifice;

(2) The mass flow is constant;

(3) The influence of the axial heat conduction of the pipe wall is ignored;

(4) There is no radiation heat leakage between outer tube and vacuum chamber.

Based on the above assumptions, a two-dimensional numerical model is established to calculate the temperature distribution of CHX. The network description of the numerical model is shown in Fig. 4, including high-pressure and low-pressure fluid, inner and outer wall. Through the analysis of each micro-element, the governing equations are as follows.

Outer wall:

$$\begin{aligned}&\rho_{1,i}A_{x1}\Delta x Cp_{1,i}\frac{T_{1,i}^{n+1}-T_{1,i}^{n}}{\Delta\tau}\\&=A_{x1}\lambda_{1,i}\frac{T_{1,i+1}^{n+1}+T_{1,i-1}^{n+1}-2T_{1,i}^{n+1}}{\Delta x}\\&+h_{1,i}A_{y1}\left(T_{2,i}^{n+1}-T_{1,i}^{n+1}\right)\end{aligned} \tag{11}$$

where A_x and A_y are the heat conduction area and the convective heat transfer area, respectively. Δx is the length of each microelement. $\Delta\tau$ is the time.

Low-pressure fluid:

$$\begin{aligned}&\rho_{2,i}A_{x2}\Delta x Cp_{2,i}\frac{T_{2,i}^{n+1}-T_{2,i}^{n}}{\Delta\tau}\\&=A_{x2}\lambda_{2,i}\frac{T_{2,i+1}^{n+1}+T_{2,i-1}^{n+1}-2T_{2,i}^{n+1}}{\Delta x}\\&+h_{1,i}A_{y1}\left(T_{1,i}^{n+1}-T_{2,i}^{n+1}\right)+h_{1,i}A_{y2}\left(T_{3,i}^{n+1}-T_{2,i}^{n+1}\right)\\&+u_{2,i}Cp_{2,i}A_{x2}\left(\rho_{2,i+1}T_{2,i+1}^{n+1}-\rho_{2,i}T_{2,i}^{n+1}\right)\end{aligned} \tag{12}$$

$$\begin{aligned}A_{x2}\Delta x\frac{\rho_{2,i}^{n+1}-\rho_{2,i}^{n}}{\Delta\tau}&=A_{x2}\rho_{2,i+1}^{n+1}\frac{u_{2,i+1}+u_{2,i}}{2}\\&-A_{x2}\rho_{2,i-1}^{n+1}\frac{u_{2,i-1}+u_{2,i}}{2}\end{aligned} \tag{13}$$

Inner wall:

$$\begin{aligned}&\rho_{3,i}A_{x3}\Delta x Cp_{3,i}\frac{T_{3,i}^{n+1}-T_{3,i}^{n}}{\Delta\tau}\\&=A_{x1}\lambda_{3,i}\frac{T_{3,i+1}^{n+1}+T_{3,i-1}^{n+1}-2T_{3,i}^{n+1}}{\Delta x}\\&+h_{1,i}A_{y2}\left(T_{2,i}^{n+1}-T_{3,i}^{n+1}\right)+h_{2,i}A_{y1}\left(T_{4,i}^{n+1}-T_{3,i}^{n+1}\right)\end{aligned} \tag{14}$$

High-pressure fluid:

$$\begin{aligned}&\rho_{4,i}A_{x4}\Delta x Cp_{4,i}\frac{T_{4,i}^{n+1}-T_{4,i}^{n}}{\Delta\tau}\\&=A_{x4}\lambda_{4,i}\frac{T_{4,i+1}^{n+1}+T_{4,i-1}^{n+1}-2T_{4,i}^{n+1}}{\Delta x}\\&+h_{2,i}A_{y3}\left(T_{3,i}^{n+1}-T_{4,i}^{n+1}\right)\\&+u_{4,i}Cp_{4,i}A_{x2}\left(\rho_{4,i-1}T_{4,i-1}^{n+1}-\rho_{4,i}T_{4,i}^{n+1}\right)\end{aligned} \tag{15}$$

$$\begin{aligned}A_{x4}\Delta x\frac{\rho_{4,i}^{n+1}-\rho_{4,i}^{n}}{\Delta\tau}&=A_{x4}\rho_{4,i-1}^{n+1}\frac{u_{4,i-1}+u_{4,i}}{2}\\&-A_{x4}\rho_{4,i+1}^{n+1}\frac{u_{4,i+1}+u_{4,i}}{2}\end{aligned} \tag{16}$$

In the energy equation of high-pressure and low-pressure fluid, the convective heat transfer coefficient is determined by the Nusselt number Nu. Nu is a geometry dependent parameter, which for the inner tube

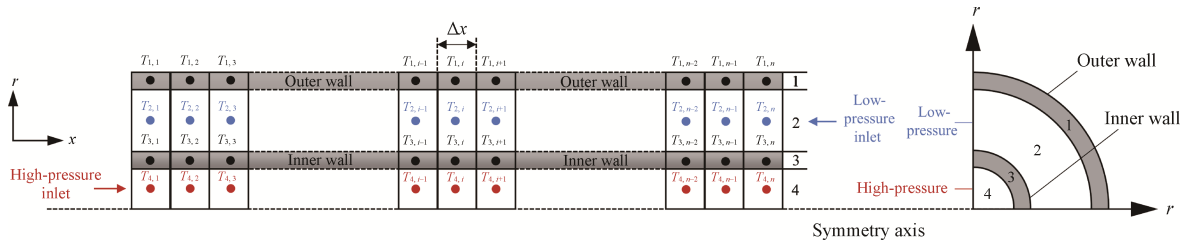

Fig. 4 Two-dimensional schematic of the nodal and control volume network, reprinted from Ref. [27]

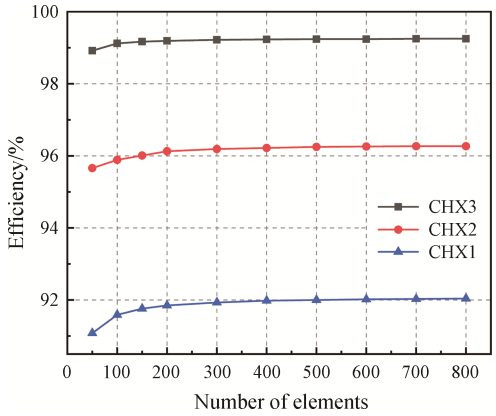

Fig. 5 Sensitivity analysis for the number of volume elements

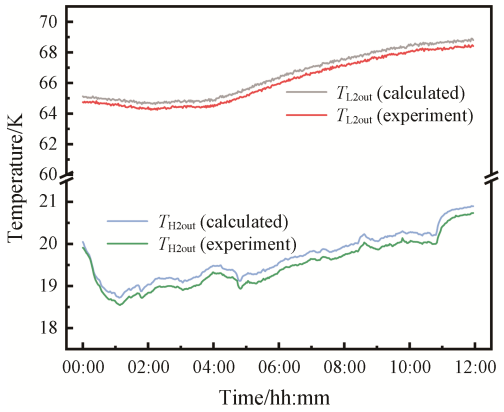

Fig. 6 CHX model validation

(high-pressure fluid flow channel) and the outer tube (low-pressure fluid flow channel) of CHX are defined as:

Inner tube [28]:

$$Nu_{in} = 0.006\ 19 Re^{0.92} Pr_{in}^{0.4} \left(1 + 3.455 \frac{d_{in}}{D_{in}}\right) \quad (17)$$

Outer tube [29]:

$$Nu_{out} = 0.0456 \left(\frac{d_{out}}{D_{out}}\right)^{0.16} Re^{0.8} Pr^{0.4} \quad (18)$$

As the most critical step of the CHX model, a model sensitivity study to the number of volume elements (N) is performed. Fig. 5 shows the variation of the effectiveness with the number of elements for a given design. Above N≈400 elements, the efficiency no longer experiences a significant change. Therefore, in the further studies N is set to 400–500.

To verify the accuracy of the CHX model, this paper uses the experimental data of the inlet temperature of the fluid in the CHX at high and low pressure at each time node as the boundary conditions and calculates the CHX outlet temperature of the fluid at high and low pressure through the CHX model. By comparing the calculated data with the experimental data, the accuracy of the CHX model is verified. Fig. 6 shows the calculated and experimental temperature curve of the high-pressure outlet and low-pressure outlet of CHX2 in 12 h. The uncertainty between the calculated value and the experimental value of the CHX model is given by the following equation:

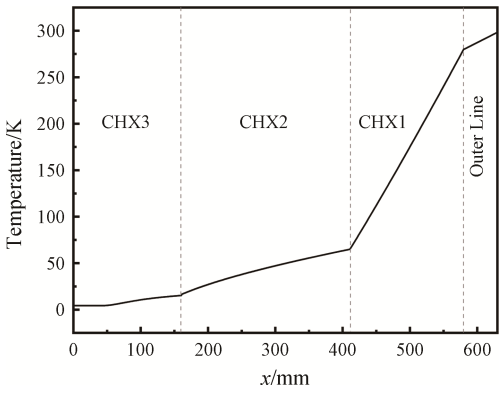

Fig. 7 Temperature distribution at t=0 h

$$\sigma = \frac{\sum_{i=1}^{n} \frac{\left|T_{cal} - T_{exp}\right|}{T_{exp}}}{n} \times 100\% \quad (19)$$

The uncertainty between the calculated temperature and experimental temperature at low-pressure outlet and high-pressure outlet is $\sigma_{T_{L2out}}$ and $\sigma_{T_{H2out}}$ respectively, which shows that the CHX model is more accurate and can be used for the calculation of CHX temperature distribution in JTC.

Based on the verified CHX model, this paper calculates the temperature distribution of the low-pressure pipeline in the CHX at t=0 h as shown in Fig. 7, where x=0 mm represents the CHX3 low-pressure inlet, and x=630 mm represents the compressor's

low-pressure inlet. By comparing the temperature distribution of CHX at each stage in the figure, it is found that the temperature distribution of CHX1 and outer line in the higher temperature region is approximately linear, while the temperature distribution of CHX2 and CHX3 in the low temperature region is nonlinear. This is mainly related to the change of helium heat capacity at low temperature. There is an isothermal zone in the CHX3 inlet section. This is mainly because the CHX3 low-pressure inlet is usually a two-phase flow. The liquid helium exchanges heat at the inlet section with latent heat, so the temperature remains unchanged.

4.2 The effect of temperature fluctuation with each stage

According to the temperature distribution given by the CHX model, the calculated $\overline{T}_L$ is shown in Fig. 8. By comparing with the temperature curve of T_{pre2}, it can be found that not only the change trend of $\overline{T}_L$ is similar to that of T_{pre2}, but also the numerical value is similar, indicating that the change of the T_{pre2} has a greater impact on the $\overline{T}_L$. In addition, it can also be found that $\overline{T}_L$ change slope in the time of 5–12 h is greater than T_{pre2}. Comparing with the temperature change curves of other stage in Fig. 2, it can be seen that the reason why the slope of $\overline{T}_L$ is greater than that of T_{pre2} in the time of 5–12 h is that the temperature of T_{pre1} and T_{atm} has increased during this period, which indicates that the T_{pre1} and T_{atm} also have an influence on $\overline{T}_L$.

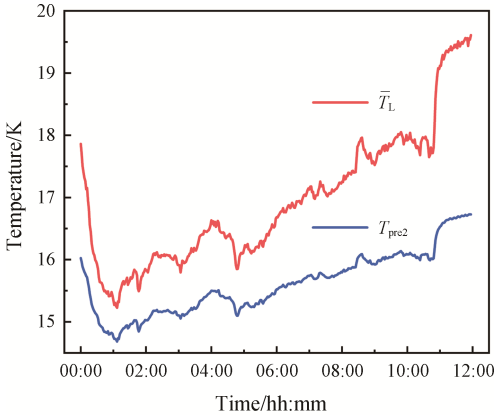

Fig. 8 Temperature change of $\overline{T}_L$ and T_{pre2}

Fig. 9 shows the amount of substance and temperature distribution in the low-pressure pipeline. It can be seen from the figure that n_L is mainly concentrated in the low temperature region, which is the temperature zone where T_{pre2} is located. This is mainly due to the increased density of helium at low temperatures so there are more substances in the low temperature region. It can be seen from Eq. (10) that $\overline{T}_L$ is related to the distribution of the amount of substance in the low-pressure pipeline, so $\overline{T}_L$ is closer to T_{pre2}. Fig. 10 shows the quantitative analysis of temperature changes at each stage on T_e when n_L=0.05 mol. From the figure, we can see that the temperature changes of the low-temperature level under the same temperature change have the greatest impact on T_e. So, according to this characteristic, the temperature control of T_{pre2} can reduce the change of T_e, which will effectively suppress the temperature fluctuation of the JTC evaporator.

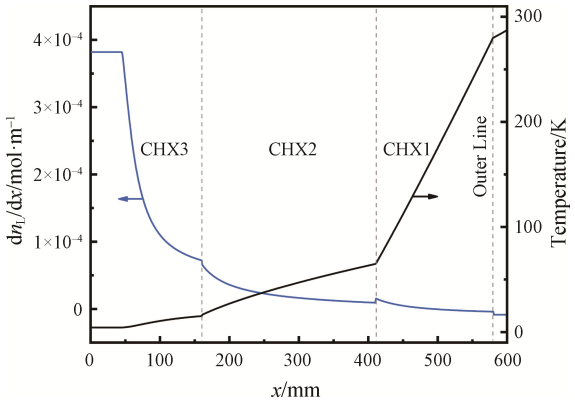

Fig. 9 dn_L/dx and temperature distribution at t=0 h

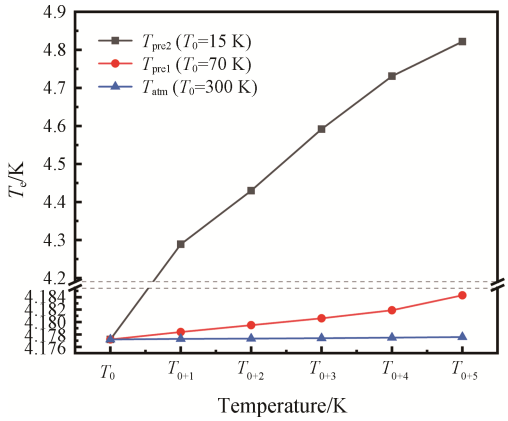

Fig. 10 The influence of temperature changes at each stage on T_e

4.3 The effect of the V_b on reducing temperature fluctuations

Fig. 11 shows the change curve of n during the experiment. Comparing with the $\overline{T}_L$ in Fig. 8, we can find that not only n_L and n_H but also their sum has an opposite trend to $\overline{T}_L$ during the experiment. In addition, we can also find that the total n in high-pressure and low-pressure pipelines will change as $\overline{T}_L$ changes. The main reason for this trend is that in addition to the V_H and V_L in the JTC system, the buffer tank in the JTC compressor unit has a volume V_b.

Therefore, as P_H and P_L change, there is a transfer of the n between the JTC pipelines and the JTC compressor unit. According to the equation of state, the characteristic that n_L is opposite to the $\overline{T}_L$ change trend is beneficial to suppress the pressure change in the low-pressure pipeline. If the JTC compressor unit does not have a buffer tank, as the $\overline{T}_L$ changes, the n_L and n_H are difficult to transfer to other parts of the JTC system, and the pressure change of P_L is greater than that of the JTC with gas reservoir. Fig. 12 shows the change trend of P_L under different V_b with the increase of $\overline{T}_L$ under the same initial working condition. With the increase of V_b, the influence of $\overline{T}_L$ change on the P_L gradually becomes smaller, especially when the V_b is much larger than V_L, the $\overline{T}_L$ change has almost no effect on the P_L. This trend is not difficult to analyze. When V_b gradually tends to infinity, the closed JT system can be regarded as an open-cycle JT system. In the open JTC, the main factors that affect the P_L are the pipeline pressure drop and the environmental pressure. The temperature change of the low-pressure pipeline has no effect on the P_L. Therefore, as the V_b gradually increases, the influence of the $\overline{T}_L$ change on P_L gradually decreases. Based on this characteristic of the closed JTC and considering the weight and volume requirements of actual applications (such as space applications), V_b of the JTC compressor unit gas reservoir can be appropriately increased to reduce the influence of the $\overline{T}_L$ change on the P_L change, thereby reducing the temperature fluctuation of the JTC evaporator.

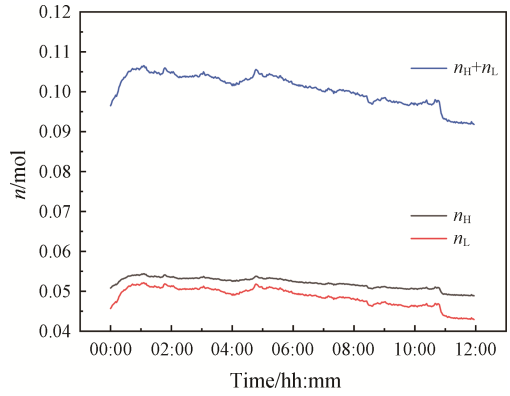

Fig. 11 The trend of n_L and n_H calculated from experimental data

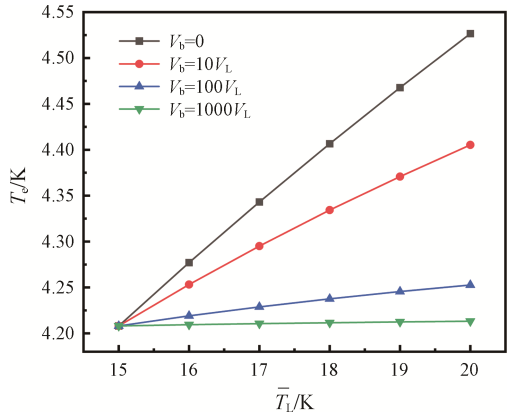

Fig. 12 The influence of V_b on T_e

5. Conclusions

Based on the two-stage GM precooler precooling the JTC, this paper carried out an experimental study on the temperature fluctuation characteristics of the JTC evaporator and analyzed the interaction influence of temperature changes among each stage on the T_e. The results showed that the fluctuation of T_{pre2} has the greatest influence on the temperature fluctuation of the JTC evaporator. At the same time, the influence of JT compressor's buffer tank volume on the P_L is analyzed. The analysis results show that increasing the V_b is beneficial to reduce the fluctuation of P_L. Based on the experimental results and the theoretical analysis, this paper discussed two methods in controlling the temperature fluctuation at the evaporator, respectively:

Active temperature control: Control the temperature of the precooler, of which the temperature control of T_{pre2} is particularly critical. Active temperature control at each stage can effectively reduce the $\overline{T}_L$ change. For example, when T_{pre2} is 17.5 K (±2.5 K), the temperature control can effectively reduce the change of T_e by about 0.6 K.

Passive temperature control: As the $\overline{T}_L$ changes, the n_L will be transferred to the JTC compressor unit. Based on this feature, the V_b can be increased to reduce the impact of the $\overline{T}_L$ change on the P_L and realize the passive control of JTC evaporator temperature fluctuation. In the device in this article, when V_b=1000 V_L the $\overline{T}_L$ change has almost no effect on T_e, so that the stability of the JTC temperature can be ensured. This is mainly because when V_b is much larger than V_L, the closed-cycle JT system can be regarded as an open-cycle JT system. However, V_b cannot be increased indefinitely due to the limitation of the volume and weight of the detector. Therefore, it is necessary to select a suitable V_b in space applications.

Acknowledgments

This study is financially supported by the Hundred Talents Program of the Chinese Academy of Sciences, the National Natural Science Foundation of China (No. 51806231), the Strategic Priority Research Program of Chinese Academy of Sciences (XDB35000000), the Natural Science Foundation of Shanghai (No.

18ZR1445600), the China Postdoctoral Science Foundation (2018M630476).

Conflict of Interest

On behalf of all authors, the corresponding author states that there is no conflict of interest.

References

[1] Ross Jr R., Boyle R., Kittel P., NASA space cryocooler programs—a 2003 overview. AIP Conference Proceedings, 2004, 710(1): 1197–1204.

[2] Coulter D.R., Ross Jr R.G., Boyle R.F., et al., NASA advanced cyrocooler technology development program. Proceeding SPIE 4850, IR Space Telescopes and Instruments, 2003, 4850: 1020–1028. DOI: https://doi.org/10.1117/12.462788

[3] Wang B., Gan Z.H., A critical review of liquid helium temperature high frequency pulse tube cryocoolers for space applications. Progress in Aerospace Sciences, 2013, 61: 43–70.

[4] Ade P.A.R., Aghanim N., Alves M.I.R., et al., Planck 2013 results. I. Overview of products and scientific results. Astronomy & Astrophysics, 2014, 571: A1.

[5] Bradshaw T.W., Orlowska A.H., Technology developments on the 4 K cooling system for "Planck" and FIRST. 6th European Symposium on Space Environmental Control Systems, Noordwijk, Netherlands, 1997, 400: 465–470.

[6] Shinozaki K., Ogawa H., Nakagawa T., et al., Mechanical cooler system for the next-generation infrared space telescope SPICA. Space Telescopes and Instrumentation 2016: Optical, Infrared, and Millimeter Wave, Edinburgh, United Kingdom, 2016, 9904: 1276–1283.

[7] Banks K., Larson M., Aymergen C., et al., James webb space telescope mid-infrared instrument cooler systems engineering. Proceeding SPIE 7017, Modeling, Systems Engineering, and Project Management for Astronomy III, Marseille, France, 2008, 7017: 93–102. DOI: https://doi.org/10.1117/12.791925

[8] Lamarre J.M., Puget J.L., Ade P.A.R., et al., Planck pre-launch status: The HFI instrument, from specification to actual performance. Astronomy & Astrophysics, 2010, 520: A9.

[9] Lundquist R.A., Balzano V., Davila P., et al., Status of the James Webb Space Telescope integrated science instrument module. Space Telescopes and Instrumentation 2012: Optical, Infrared, and Millimeter Wave, Amsterdam, Netherlands, 2012, 8442: 947–972.

[10] Orlowska A.H., Bradshaw T.W., Hieatt J., Development status of a 2.5 K–4 K closed-cycle cooler suitable for space use. Cryocoolers, 1995, 8: 517–524.

[11] Inatani J., Narasaki K., Tsunematsu S., et al., Mechanical cooler and cryostat for submillimeter SIS mixer receiver in space. Sensors, Systems, and Next-Generation Satellites V, Toulouse, France, 2001, 4540: 197–208.

[12] Narasaki K., Tsunematsu S., Yajima S., et al., Development of cryogenic system for SMILES. AIP Conference Proceedings, 2004, 710(1): 1785–1796.

[13] Prouvé T., Duval J.M., Charles I., et al., Athena X-IFU 300 K–50 mK cryochain demonstrator cryostat. Cryogenics, 2018, 89: 85–94.

[14] Liu S., Sha X., Ding L., Investigation of the frequency and stroke characteristics of two-stage valved linear compressor in a 4 K JT cryocooler. Applied Thermal Engineering, 2020, 176: 115432.

[15] Hasegawa Y., Nakamura D., Murata M., et al., High-precision temperature control and stabilization using a cryocooler. Review of Scientific Instruments, 2010, 81(9): 094901.

[16] Nakamura D., Hasegawa Y., Murata M., et al., Reduction of temperature fluctuation within low temperature region using a cryocooler. Review of Scientific Instruments, 2011, 82(4): 044903.

[17] Jambusaria M.H., Burkic A.A., Ellis M.J., et al., Microsat cryocooler system. Infrared Technology and Applications XLI, Maryland, United States, 2015, 9451: 549–561.

[18] Freeman J.J., Murphy J.B., Kirkconnell C.S., Experimental demonstration of cryocooler electronics with multiple mechanical cryocooler types. Infrared Technology and Applications XXXVIII, Maryland, United States, 2012, 8353: 668–679.

[19] Ding L., Zhang H., Sha X., et al., Study on the establishing-process of piston offset in the helium valved linear compressor under different operating parameters. International Journal of Refrigeration, 2022, 133: 80–89.

[20] Narasaki K., Tsunematsu S., Ootsuka K., et al., Development of 1 K-class mechanical cooler for SPICA. Cryogenics, 2004, 44(6–8): 375–381.

[21] Crook M., Bradshaw T., Gilley G., et al., Development of a 2 K Joule-Thomson closed-cycle cryocooler. Cryocoolers, 2016, 19: 9–18.

[22] Maytal B.Z., Pfotenhauer J.M., Miniature Joule-Thomson cryocooling: principles and practice. Springer Science & Business Media, New York, 2012.

[23] Chen Z., Liu S., Wu Y., et al., Performance testing and temperature fluctuations of a 4.5 K@ 150 mW Joule-Thomson closed cycle cryocooler for space applications. IOP Conference Series: Materials Science and Engineering, 2022, 1240(1): 012017.

[24] Van Sciver S.W., Timmerhaus K.D., Clark A.F., Helium cryogenics. Springer Science & Business Media, New

York, 2012.

[25] Ortiz Vega D.O., A new wide range equation of state for helium-4. Texas A & M University, Texas, United States, 2013.

[26] Onufrena A., Koettig T., Bremer J., et al., Design of a compact mesh-based high-effectiveness counter-flow heat exchanger and its integration in remote cooling systems. International Journal of Heat and Mass Transfer, 2022, 183: 122107.

[27] Chen Z., Cui X., Liu S., et al., Study on cooling capacity characteristics of a helium Joule-Thomson cryocooler. Applied Thermal Engineering, 2023, 221: 119820.

[28] Xin R.C., Ebadian M.A., The effects of Prandtl numbers on local and average convective heat transfer characteristics in helical pipes. ASME Journal of Heat and Mass Transfer, 1997, 119(3): 467–473.

[29] Hardik B.K., Baburajan P.K., Prabhu S.V., Local heat transfer coefficient in helical coils with single phase flow. International Journal of Heat and Mass Transfer, 2015, 89: 522–538.